

Milford et al. 1989

acid, 373-49-9; myristic acid, 544-53-8.

## Literature Cited

- (1) Schecter, A.; Dekin, A.; Weerasinghe, N. C. A.; Arghestani, S.; Gross, M. L. *Chemosphere* 1988, 17, 627.
- (2) Bumb, R. R.; Crumett, W. B.; Cutie, S. S.; Gledhill, J. R.; Hummel, R. H.; Kagei, R. O.; Lamparski, L. L.; Luoma, E. V.; Miller, D. L.; Nestruck, T. J.; Shadoff, L. A.; Stehl, R. H.; Woods, J. S. *Science* 1983, 210, 385.
- (3) Czuczwa, J. M.; McBeety, B. D.; Hites, R. A. *Science* 1984, 226, 568.
- (4) Czuczwa, J. M.; Hites, R. A. *Chemosphere* 1986, 15, 1417.
- (5) Cockburn, A.; Barraco, R. A.; Reyman, T. A.; Peck, W. H. *Science* 1975, 187, 1155.

- (6) Patterson, D. G.; Holler, J. S.; Lapeza, C. R.; Alexander, L. R.; Groce, D. F.; O'Conner, R. C.; Smith, S. J.; Liddle, J. A.; Needham, L. L. *Anal. Chem.* 1986, 58, 705.
- (7) Feng, Z.-C.; Huangfu, Y.-M.; Huang, Z.-J.; Chai, X.-L.; Long, F.-O. *Wuhan I Hsueh Yuan Hsueh Pao* 1980, 9, 11.
- (8) Smith, G. *Discover* 1986, October, 72.
- (9) Skelly, E. Proceedings of the 27th Eastern Analytical Symposium, October 2-7, 1988; paper 253.
- (10) White, A.; Handler, P.; Smith, E. L. *Principles of Biochemistry*; McGraw Hill: New York, 1973; p 68.
- (11) Karasek, F. W.; Dickson, L. C. *Science* 1987, 237, 754.

Received for review January 6, 1989. Revised manuscript received May 17, 1989. Accepted June 27, 1989.

## A New Approach to Photochemical Pollution Control: Implications of Spatial Patterns in Pollutant Responses to Reductions in Nitrogen Oxides and Reactive Organic Gas Emissions

Jana B. Milford,<sup>†</sup> Armistead G. Russell,<sup>‡</sup> and Gregory J. McRae<sup>\*§</sup>

Department of Engineering and Public Policy, Carnegie Mellon University, Pittsburgh, Pennsylvania 15213

■ This analysis addresses whether nitrogen oxides (NO<sub>x</sub>) emissions controls should be used in addition to reductions of reactive organic gases (ROG), and what measures of air quality should be used to evaluate alternative strategies. The results of this study call into question the adequacy of control strategies that rely exclusively on ROG emissions reductions. Based on the predictions of an Eulerian photochemical model for a 2-day episode in August 1982, distinctly different combinations of NO<sub>x</sub> and ROG reductions appear to be most effective in lowering photochemical pollutant levels at different locations within the Los Angeles basin. For example, while peak ozone concentrations at some locations were predicted to increase with reduced NO<sub>x</sub> emissions, reductions in NO<sub>x</sub> were predicted to be required in order to meet the National Ambient Air Quality Standard (NAAQS) for ozone at downwind locations. Similarly conflicting responses were predicted for inorganic nitrate and peroxyacetyl nitrate (PAN). As base case concentrations of radicals and the ratio of ROG to NO<sub>x</sub> increased downwind of strong source areas, the amount of improvement in air quality that could be achieved by reducing NO<sub>x</sub> emissions generally increased, while the efficacy of ROG controls decreased.

### 1. Introduction

More than half of the people living in the United States reside in areas where ozone concentrations exceed the National Ambient Air Quality Standard (NAAQS). Additionally, some urban areas such as Los Angeles are also out of compliance with standards for particulate matter (PM<sub>10</sub>). Given that the nation currently spends more than \$30 billion per year on air pollution controls, there is an urgent need to identify new control options (1). As the current widespread lack of compliance is coupled with the prospect of an even more stringent standard arising from recent studies that suggest that, as set at 0.12 ppm (1-h average), the ozone standard leaves little or no margin of protection against human health effects (2-4), it is clear that the challenge facing air pollution control agencies is

particularly difficult. In fact, many agencies already feel that they have exhausted the technical, political, and economically feasible control measures available to address the problem (5, 6). To further complicate the issue, it is becoming increasingly apparent that the problem of photochemical air pollution extends beyond individual cities. Suburban and rural areas are being impacted by ozone and other reaction products produced in upwind areas and transported over hundreds of kilometers (7). In addition to high ozone levels, there are also cooccurring air pollution problems of toxic species, acid deposition, and visibility degradation. In short, the time has arrived for a critical reassessment of present approaches to controlling photochemical oxidant air pollution.

Current control efforts are focused on ensuring that the highest ozone concentrations in urban areas are below the standard. Air quality objectives related to other pollutants or to rural areas are presently assumed either to be relatively unimportant or to be consistent with the goal of attaining the ozone standard. Controls on emissions of reactive organic gases (ROG), rather than nitrogen oxides (NO<sub>x</sub>), have generally been relied on to reduce peak ozone concentrations (8). In the case of photochemical air pollution, the question of whether to reduce NO<sub>x</sub> or ROG emissions, or both, is greatly complicated by the fact that the impacts of the reductions might not be spatially uniform. For example, NO<sub>x</sub> emissions may suppress ozone formation in the immediate vicinity of a large source, but enhance downwind ozone formation. Differences in impacts across locations and pollutants are problematic because they preclude the identification of a single, "optimal" control strategy. The main point of this paper is that if progress is to be made in improving photochemical air quality, the following elements must be considered in the planning process: (1) multiple air quality objectives, (2) the effects of emissions controls on pollutants other than ozone, and (3) spatial patterns and overall population exposure to air pollution.

### 2. Traditional Methods for Designing Photochemical Oxidant Control Strategies

The problem of determining local control requirements to reduce photochemical air pollution has usually been defined in terms of establishing the ROG emissions control

<sup>†</sup> Current address: Department of Civil Engineering, University of Connecticut, Storrs, CT 06269.

<sup>‡</sup> Department of Mechanical Engineering.

<sup>§</sup> Departments of Chemical Engineering and Engineering and Public Policy.

level required to reduce the maximum observed ozone concentrations to below the NAAQS. In this approach, the objective is to minimize the cost of emissions controls subject to meeting an air quality goal. Stated as a mathematical programming problem, the design problem becomes

$$\text{Min cost } [\Delta E_{\text{ROG}}(\mathbf{x}, t)] \quad (1)$$

$$\{E_{\text{ROG}}(\mathbf{x}, t)\}$$

subject to

$$\text{Max } [O_3\{E_{\text{NO}_x}, E_{\text{ROG}}, \mathbf{x}, t\}] \leq 0.12 \text{ ppm} \quad (2)$$

where  $E_{\text{ROG}}$  and  $E_{\text{NO}_x}$  are the emissions levels corresponding to the set of feasible control strategies, and  $\Delta E_{\text{ROG}}$  represents the reduction of ROG emissions from the base case, and (2) represents the constraint that the maximum ozone concentration anywhere inside the airshed must be less than the standard. A similar statement could be developed for meeting other air quality standards, such as for  $\text{NO}_2$  and  $\text{PM}_{10}$ . Although simply stated, the formulation (1, 2) hides a number of difficulties including the fact that there may be no technical or politically feasible solutions. At the heart of the control strategy design problem is the need for an accurate emissions-air quality relationship that can be used to test the proposed strategies against constraint 2. The most widely used approach to estimating emissions reduction requirements is the Empirical Kinetics Modeling Approach (EKMA) (9). Based on a simplified, single-cell trajectory formulation, the EKMA model has been designed to predict peak ozone concentrations corresponding to a large number of ROG and  $\text{NO}_x$  reduction combinations. The level of ROG reductions required to move from the observed ozone concentration to the standard is then estimated from a response surface diagram or isopleth developed from the modeling results.

A principal justification for the traditional focus on ROG controls has been a concern (consistently supported by experiments and modeling) that reducing  $\text{NO}_x$  emissions could, under some circumstances, increase ozone concentrations at some locations (8). However, recent measurements of ROG and  $\text{NO}_x$  concentrations in a number of areas (10), new modeling analyses (11, 12), and new estimates of the impact of ROG emissions from vegetation (12-14) have led to the need to reassess the basic approach for lowering ozone. In fact, in its post-1987 policy proposal, the U.S. EPA has suggested that some areas may be required to consider  $\text{NO}_x$  in addition to ROG controls (15).

Furthermore, it is not clear whether peak ozone concentrations observed within the urban area are the best measures of air quality for use in designing control strategies (8). If the control strategy design formulation (1, 2) is extended to include gas-phase pollutants other than ozone, and key components of  $\text{PM}_{10}$  (the ambient air quality standard for particulate matter less than  $10 \mu\text{m}$  in diameter) like aerosol nitrate, then the EKMA approach is clearly not adequate. With its simplified treatment of the underlying physical and chemical processes, EKMA is not capable of correctly accounting for pollutant carryover during multiday pollution episodes, or being tested against observed air quality. From a control strategy design point of view, EKMA is unfortunately extremely sensitive to initial and boundary conditions (16). Finally, a major flaw in the traditional approach is the implicit assumption that controls developed to reduce the peak ozone to below the standard are sufficient to ensure compliance over the whole airshed. Numerous modeling studies have shown how the effects of emissions controls can vary within an airshed (17-19). In fact, this complication has been a major rationale for the development and use of Eulerian models capable of predicting the air quality

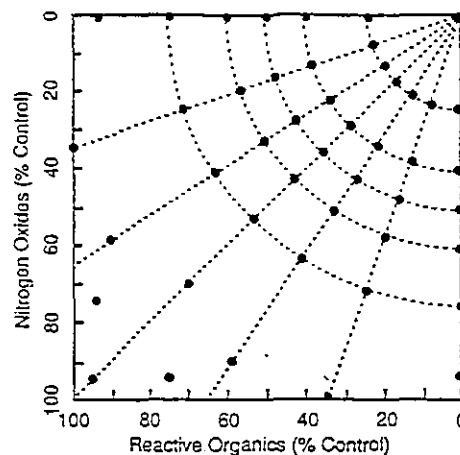


Figure 1. ROG and  $\text{NO}_x$  emissions reduction combinations (●) for which air quality calculations were performed. The upper right-hand corner of the diagram corresponds to the 1982 base-line emissions of ROG and  $\text{NO}_x$ .

distribution over urban airsheds (20).

### 3. Use of Airshed Models To Design Emissions Control Strategies

Current photochemical airshed models are capable of calculating the evolution of pollutants in the atmosphere by accurately describing the physical and chemical processes responsible for chemical transformation, transport, and fate. In the past, because of the high computational costs associated with these models, most applications were confined to a limited number of time periods and control scenarios. Advances in computational technology now, however, enable the direct computation of control isopleths using comprehensive, spatially resolved photochemical dispersion models. This paper examines, for the first time, the effects of a comprehensive set of reductions in emissions of ROG and  $\text{NO}_x$  on the concentration distributions of ozone, peroxyacetyl nitrate (PAN), and inorganic nitrate ( $\text{NO}_3^-$ , the sum of nitric acid and ammonium nitrate) concentrations over a major metropolitan area.

More than 45 different combinations of control levels (shown in Figure 1) were used to develop concentration isopleths for locations across a 200-km-wide portion of the Los Angeles basin. Although emissions reductions greater than 80% were evaluated, by far the largest number of cases were concentrated at control levels that might be expected over the next 10 years. Each 2-day simulation using the model described in (21-23) required approximately 40 min of computer time on a CRAY X-MP/48. The model used to perform the analysis has emissions, pollutant concentrations, surface features, and meteorological parameters resolved into five vertical segments and  $25\text{-km}^2$  horizontal grid squares. Meteorological parameters, photolysis rates, and emissions vary both spatially and diurnally. Detailed descriptions of the model and the chemical reaction mechanism it contains and results of evaluations are given in (17, 21-24). While the specific calculations apply to Los Angeles, the issues and methods of this analysis are likely to be applicable to many other urban locations. For example, the time required to transport ozone and its precursors from downtown Los Angeles to the eastern edge of the basin is comparable to the scale of intercity and urban-to-rural transport of concern in the eastern United States. Furthermore, the variation in ROG and  $\text{NO}_x$  emissions levels across the region spans the levels found in other urban areas. The results presented here are thus expected to provide general insight into the implications of different air quality metrics and the relative effectiveness of ROG and  $\text{NO}_x$  controls.

Table I. Boundary Conditions for Inflow from the Pacific Ocean

species	inflow concn, ppm	
	surface	aloft
O <sub>3</sub>	0.04	0.06
NO	0.01	0.00
NO <sub>2</sub>	0.01	0.00
ROG (ppm C)	0.15	0.15

#### 4. Base Case Predictions

Before a model can be used for control strategy calculations it is critically important to demonstrate that it has the capability to accurately reproduce historical events. The South Coast Air Basin (SoCAB) surrounding Los Angeles, CA, was selected for this study because of the severity of the photochemical air pollution problem there as well as the availability of an extensive aerometric data base. The SoCAB experiences ozone concentrations in excess of 3 times the national standard, and photochemically derived aerosols contribute to PM<sub>10</sub> levels of 2-3 times the standard. The area encompasses major portions of Ventura, Los Angeles, San Bernardino, Orange, and Riverside Counties in Southern California. The modeling region extends over 200 km east-to-west and 100 km north-to-south. For this study, calculations were carried out over 48 h, with meteorological conditions and base case emissions corresponding to the period August 30-31, 1982. There are several reasons for selecting these days. The first is that moderately high photochemical smog levels were experienced throughout the Los Angeles basin over the 2-day period. On August 31, the maximum ozone concentration observed in the airshed was 0.23 ppm, recorded at the Riverside monitoring site. In fact, the August episode was recently classified as one of the two most common types of high-ozone periods in the Los Angeles area (25). The meteorological conditions were conducive to the formation of high oxidant levels since the temperatures in the area reached 37 °C and the low average wind velocity across the basin from west to east allowed overnight accumulation of pollutants. Since ozone is not the only determinant of urban air quality, and there is considerable current interest in issues associated with PM<sub>10</sub>, the primary reason for choosing the 1982 episode was because it corresponded to the only time period during which a comprehensive program was mounted to characterize particulate air quality (23).

Spatially and temporally resolved estimates of summertime, weekday ROG, NO<sub>x</sub>, and CO emissions were developed for the region. The base estimates were augmented with day-specific emissions data from major point sources. Total emissions of ROG and NO<sub>x</sub> in the modeling region were estimated at 1260 × 10<sup>3</sup> and 1120 × 10<sup>3</sup> kg day<sup>-1</sup>, respectively. While most emissions are concentrated in the central Los Angeles County area, lower but still substantial levels of ROG and NO<sub>x</sub> are emitted to the south and east into San Bernardino, Orange, and Riverside Counties. Apart from the emissions and meteorology, the other major determinants of the concentration dynamics in an urban airshed are the choices made for initial and boundary conditions. For the base case the needed data were interpolated directly from available field measurements. Table I presents the values adopted for the ocean boundary. Locating the computational boundaries well away from the extent of land-sea breeze reversals provides a way to minimize the effects of uncertainties in the values adopted for the inflow boundary conditions (22). Figure 2 illustrates the extent of penetration of air from the ocean

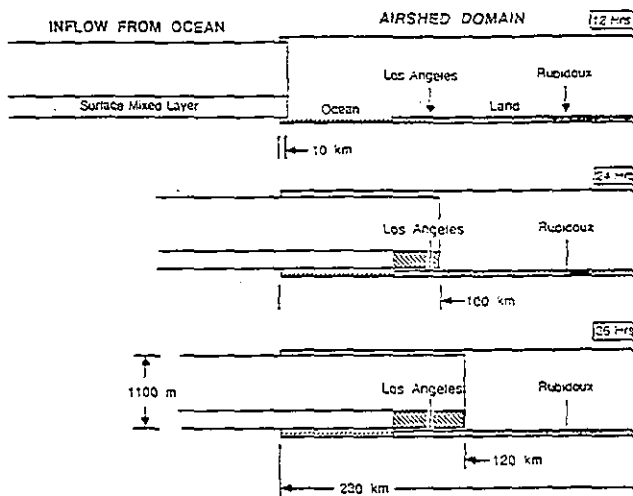


Figure 2. Schematic representation of the extent of oceanic air penetration into the airshed modeling domain. The average position of the front was derived from the full three-dimensional flow field. After 36 h the front is still more than 50 km from the location of the highest observed ozone levels. (The vertical scale and integrity of the surface mixed layer has been exaggerated for clarity.)

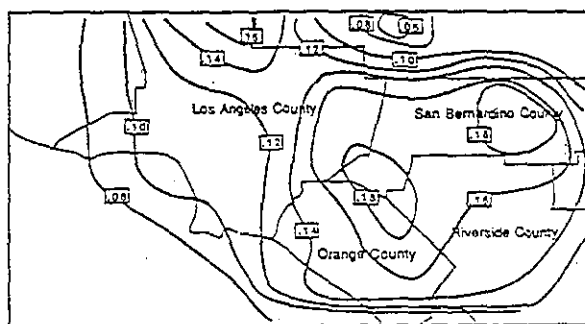


Figure 3. Distribution of predicted peak ozone concentrations (ppm) for August 31, 1982, base case.

after 36 h. The position of the front at the end of each 12-h period was derived from trajectory analyses of the underlying flow field. One particularly important feature to note is that after 36 h the front is still more than 50 km from the region of highest ozone concentrations. In other words, the choice of inflow boundary conditions has a negligible effect on the peak ozone levels. Similarly, by running the model for 2 days it is possible to significantly reduce the influence of uncertainties in the initial conditions.

Since a detailed evaluation of the performance of the model in predicting O<sub>3</sub>, NO<sub>2</sub>, HNO<sub>3</sub>, NH<sub>4</sub>NO<sub>3</sub>, and PAN concentrations during this 2-day period is available in ref 23, it will not be repeated here. In summary, however, it was found that O<sub>3</sub> and PAN concentration predictions were in excellent agreement with observations and that NO<sub>2</sub> predictions were substantially better than had been achieved in previous studies. Figure 3 shows the maximum 1-h average ozone concentrations across the Los Angeles basin on August 31, as predicted for the base case. Throughout the airshed, peak ozone concentrations exceed 0.08 ppm, with concentrations over areas east of downtown Los Angeles well above the national standard of 0.12 ppm. Peak ozone levels are highest well downwind of the dominant emissions area, consistent with observed trends. The time at which the peaks are predicted to occur shifts from midday at downtown Los Angeles to late afternoon as the main urban plume travels east across the airshed. Concentrations exceeding 0.17 ppm develop ~50 km east of downtown Los Angeles, and also ~100 km east-northeast

Figure  
emissio  
Pasade

of do  
ppm,  
The p  
distrib  
to tha  
town  
NH<sub>4</sub>N  
respec  
tions.  
excele  
case  
proce

5. Co  
Isople

Giv  
next s  
of pre

12 Hrs  
24 Hrs  
36 Hrs

panic air position  
id. After  
highest  
surface

ms (ppm)

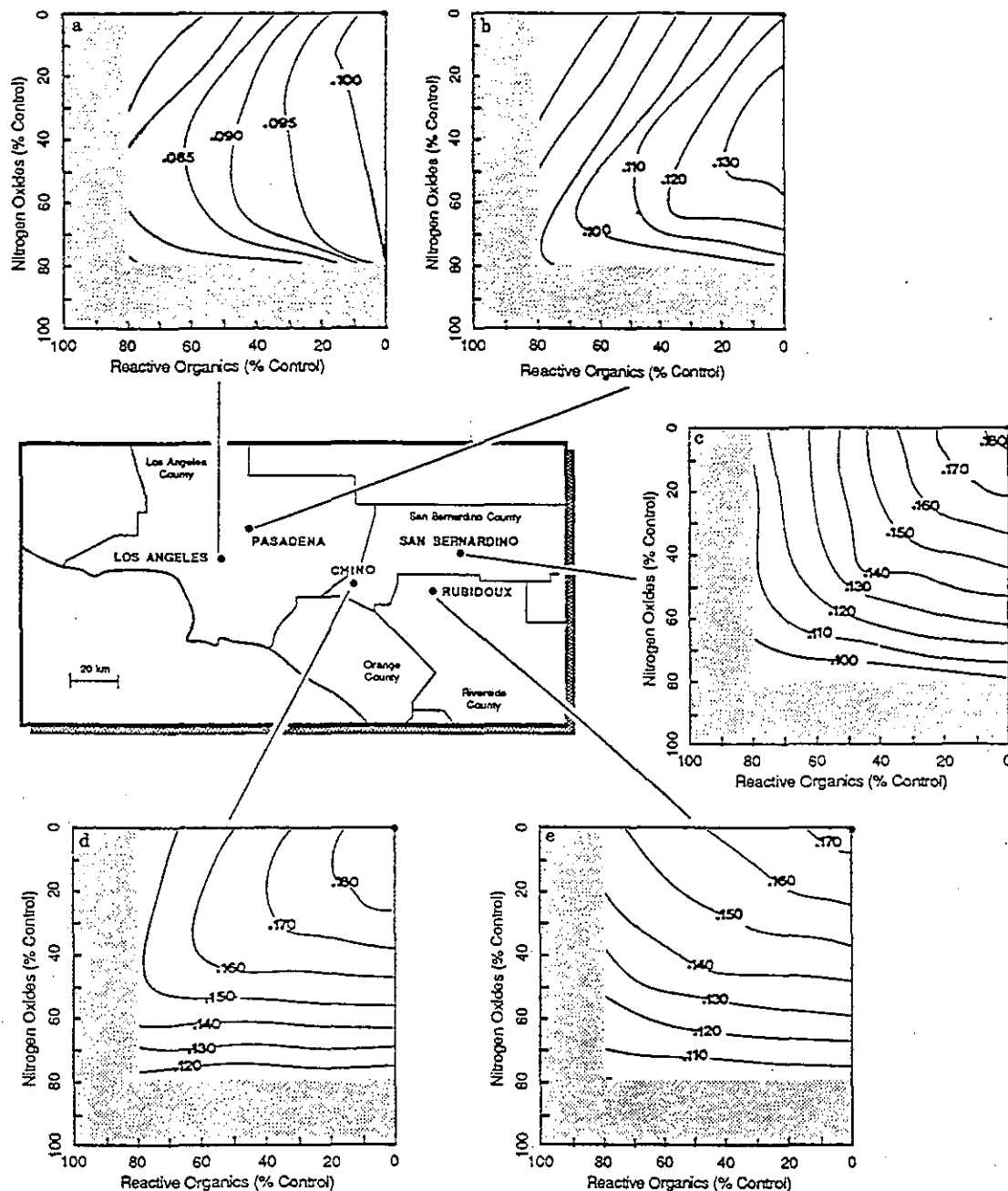


Figure 4. Predicted response of peak ozone concentrations (ppm) at locations across the Los Angeles basin, to spatially uniform  $\text{NO}_x$  and ROG emissions reductions. The upper right-hand corner of each response diagram corresponds to the base case. (a) Downtown Los Angeles; (b) Pasadena; (c) San Bernardino; (d) Chino; (e) Rubidoux.

of downtown. The highest ozone concentration is 0.20 ppm, predicted to occur at 3 p.m., near San Bernardino. The peak  $\text{HNO}_3$ ,  $\text{NH}_4\text{NO}_3$ , and PAN concentrations are distributed over the airshed in a pattern roughly similar to that of ozone, generally increasing downwind of downtown Los Angeles. The highest concentrations of  $\text{HNO}_3$ ,  $\text{NH}_4\text{NO}_3$ , and PAN predicted were 18, 27, and 14 ppb, respectively. Both the gas-phase and particulate predictions are in excellent agreement with observations. The excellent performance of the model in reproducing the base case conditions provides a viable base from which to proceed with the control strategy calculations.

### 5. Construction of Spatially Resolved Pollutant Isoleths

Given satisfactory performance for the base case, the next step was to determine the effects of differing levels of precursor controls. The objective was to develop a set

of "EKMA-like" control isopleths for different locations within the airshed. The data needed to develop the concentration contours were derived from many individual calculations, each corresponding to one of the control combinations shown in Figure 1. Emissions controls were modeled as uniform percentage reductions applied to all sources and ranged from 0 to 100% of the base-line emissions levels. Although it is easy to construct the emissions reductions, one of the major difficulties in using airshed models to test the air quality impacts of alternative control strategies is choosing appropriate initial and boundary conditions. Under conditions of drastically reduced emissions, the original ambient air quality measurements will no longer be appropriate. In this study, the initial concentrations of emitted species within the modeling region were derived by scaling the base case monitoring values in direct proportion to the emissions reductions.

Inflow concentrations along the boundary of the region

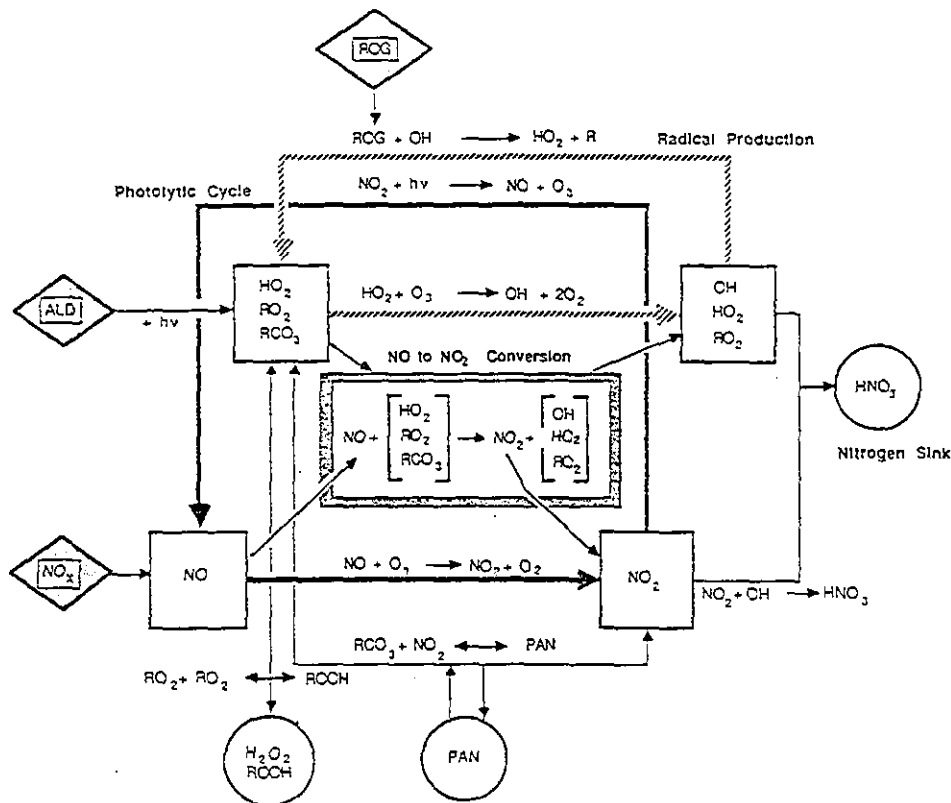


Figure 5. Schematic representation of the  $\text{NO}_x$  and radical reaction cycles involved in the production and consumption of ozone. Diamonds indicate emissions; circles indicate chemical sinks.

were not scaled. There were several reasons for this decision. As shown in the last section, the oceanic inflow boundary had a negligible effect on downwind air quality. In addition, it is not clear that future controls will have a major impact on upwind air quality. As a test of the effect of the inflow assumption, two control runs were carried out, both corresponding to 50% reductions of  $\text{NO}_x$  and ROG. In one case the inflow concentration was the same as that shown in Table I and in the other the ROG level was lowered to 10 ppb C. Under these conditions the peak ozone on the second day was only lowered by 0.1%. The fact that a 15-fold reduction in the inflow oceanic boundary condition led to such a small change in predicted air quality is a testimony to the efficacy of the procedures used to locate the computational boundaries. The more difficult decision was the treatment of inflow through the northern, land-based, boundary. At present there is no truly defensible procedure, since even under conditions of very stringent controls in the Los Angeles basin there is no guarantee that areas to the north of the region will adopt similar measures. (This problem is even more serious for eastern cities where transport times and distances between cities are very short.) In either case, for the particular conditions of this study, the peak ozone values under conditions of almost 100% control occurred on the far eastern boundary. This effect could be minimized in future studies by extending the modeling region even further to capture the flow reversals at night.

For each control combination hourly average pollutant concentrations were computed for each grid point in the modeling region. Isoleths were drawn for  $\text{O}_3$ , PAN, and  $\text{NO}_3^-$  ( $\text{HNO}_3 + \text{NH}_4\text{NO}_3$ ) at selected receptor sites across the basin by determining, for each location and control combination, the maximum concentration of each species predicted over the second 24-h period. Since the problems associated with inflow boundary conditions only became apparent at very high and currently technically infeasible control levels, we decided to present the concentration

contours for emissions reductions in the range 0-80%. As an illustration of the results, Figure 4 presents predicted responses of peak ozone concentrations to  $\text{NO}_x$  and ROG emissions reductions for selected monitoring sites. The effects of both ROG and  $\text{NO}_x$  reductions, as well as the base-line ozone concentrations, differ significantly between locations. An overall trend is apparent. Moving west to east, the sensitivity of  $\text{O}_3$  to  $\text{NO}_x$  emissions increases and the sensitivity of  $\text{O}_3$  to ROG emissions decreases. As shown in Figure 3, base-line peak ozone concentrations also increase across the modeling region. At downtown Los Angeles and Pasadena, the ozone concentrations increase with initial  $\text{NO}_x$  reduction steps, in the absence of concurrent ROG reductions. The effect is especially strong at Pasadena, where, for example, a 16% increase in  $\text{O}_3$  is predicted to result from a 35% reduction in  $\text{NO}_x$  emissions. At other locations, especially those southeast of downtown,  $\text{NO}_x$  controls appear to be more effective in reducing ozone than equivalent percentage ROG controls. Among the isopleths presented, Rubidoux provides the most extreme example, with a 35% reduction in  $\text{NO}_x$  approximately twice as effective in reducing  $\text{O}_3$  as a similar level of ROG control. The model predicts that an 80% reduction in ROG emissions is insufficient to reduce the maximum ozone concentrations to 0.12 ppm at locations such as Chino and Rubidoux. With or without ROG reductions, it appears that significant  $\text{NO}_x$  reductions are required to achieve the NAAQS under the conditions modeled.

#### 6. Interpretation of Spatial Patterns in Response to Emissions Reductions

The isopleths presented in Figure 4 exhibit separate regimes of relative insensitivity to  $\text{NO}_x$  and ROG reductions that are characteristic of ozone isopleths (26). Figure 5 shows the interaction between the  $\text{NO}_x$  and ROG reaction cycles that account for this behavior. The buildup of ozone concentrations that occurs in urban areas results

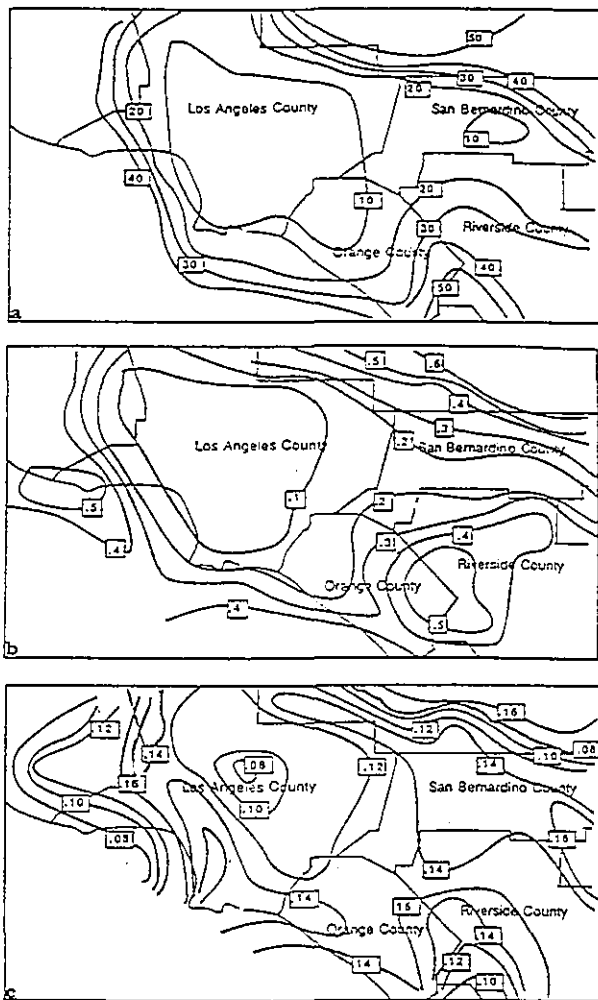


Figure 6. Distribution over the modeling region of predicted base case values of (a)  $\text{ROG}/\text{NO}_x$  (ppm C/ppm) at 9 a.m., (b)  $\text{HO}_2 \times 10^{-4}$  (ppm) at noon, and (c)  $\text{OH} \times 10^{-8}$  (ppm) at noon.

from enhancement of the rate of ozone production by photolysis of  $\text{NO}_2$  over the rate of ozone consumption by its reaction with  $\text{NO}$ . This enhancement occurs when peroxy radicals, rather than ozone, oxidize  $\text{NO}$  to  $\text{NO}_2$ . The peroxy radical ( $\text{RCO}_2, \text{RO}_2, \text{HO}_2$ ) +  $\text{NO}$  reactions link the  $\text{NO}_x$  cycle with the ROG cycle. Reactive organics produce peroxy radicals via reaction with hydroxyl radicals, and by photolysis, in the case of aldehydes.

The upper left portions of ozone isopleths correspond to  $\text{NO}_x$ -rich systems, in which peak ozone concentrations may decrease if  $\text{NO}_x$  emissions increase. In such systems, radical and ozone concentrations are suppressed by the addition of  $\text{NO}_x$ . The dominant loss mechanism for radicals under  $\text{NO}_x$ -rich conditions is the reaction of  $\text{OH}$  radicals and  $\text{NO}_2$  to produce  $\text{HNO}_3$ . This loss of hydroxyl radicals reduces ROG oxidation. ROG concentrations are too low in these systems to propagate radicals through the cycle by competing against the  $\text{HNO}_3$  formation reaction. The decrease in peroxy radical production that occurs when  $\text{NO}_x$  is added results in lower ozone concentrations as less  $\text{NO}$  is oxidized by reaction with peroxy radicals rather than ozone. In  $\text{NO}_x$ -rich systems, reducing ROG emissions reduces radical generation by aldehyde photolysis as well as radical cycling, resulting in decreased peroxy radical production and consequently lower ozone concentrations.

In the ROG-rich systems represented by the lower right portions of typical isopleths, reductions in  $\text{NO}_x$  emissions decrease net ozone production, while little change is affected by ROG emissions reductions. In this case con-

centrations of ROG are high enough to produce a relative excess of peroxy radicals. It is the  $\text{NO}$  concentration that limits the rate of the peroxy radical- $\text{NO}$  reactions, thus limiting ozone production as well as further cycling of radicals. While high peroxy radical concentrations could potentially deplete ozone through the reaction of  $\text{HO}_2$  with  $\text{O}_3$ , the effect of this reaction is limited as it competes with termination reactions between peroxy radicals, such as the reaction of two hydroperoxy radicals to form hydrogen peroxide. Finally, as ROG concentrations increase relative to  $\text{NO}_2$  levels, the balance between peroxy and hydroxyl radicals is shifted in favor of peroxy radicals, and consequently PAN production increases in importance relative to  $\text{HNO}_3$  production.

Figure 6a shows the  $\text{ROG}/\text{NO}_x$  ratios predicted across the airshed for the base case at 9 a.m., indicating the distribution prior to extensive reaction and downwind transport.  $\text{NO}_x$  has been calculated as the sum of  $\text{NO}$  and  $\text{NO}_2$  to represent the component of total  $\text{NO}_x$  that is active in the production and consumption of ozone. The values shown are thus not strictly comparable to  $\text{NO}_x$  measurements, which can include significant contributions from PAN and  $\text{HNO}_3$ . (The distinction is expected to be negligible early in the day, but to increase in importance as concentrations of  $\text{HNO}_3$  and PAN build up while those of  $\text{NO}_2$  and  $\text{NO}$  decline.) The  $\text{NO}_x$  concentrations predicted for 9 a.m. range from  $\sim 0.2$  ppm over the center of Los Angeles County to less than 0.02 ppm at the eastern edge of the modeling region. ROG concentrations range from about 2–0.3 ppm C over the same area. The ratios of ROG to  $\text{NO}_x$  predicted for 9 a.m. fall between 5 and 10 ppm C/ppm over most of Los Angeles County and range to higher than 30 ppm C/ppm over San Bernardino and Riverside Counties. By comparison, the measured values of  $\text{ROG}/\text{NO}_x$  were approximately 5 ppm C/ppm within  $\sim 30$  km of downtown Los Angeles at 9 a.m. on August 31, in close agreement with predictions. By noon, when elevated concentrations of  $\text{O}_3$ , PAN, and  $\text{NO}_3^-$  have developed, the predicted ROG to  $\text{NO}_x$  ratios have approximately doubled at most locations, due primarily to reduced  $\text{NO}$  and  $\text{NO}_2$  concentrations. As shown in Figure 6, parts b and c, and as might be expected from the discussion of radical cycling, the contours of predicted hydroxyl and hydroperoxy radicals generally follow the  $\text{ROG}/\text{NO}_x$  ratios.

The differences in the shapes of the isopleth diagrams in Figure 4 follow from the distributions of ROG,  $\text{NO}_x$ , and radical species. As suggested by the concentrations of ROG and  $\text{NO}_x$  in the area at 9 a.m., Pasadena is within the region of high emissions. At noon, the predicted value of  $\text{ROG}/\text{NO}_x$  is only 9.0 ppm C/ppm, further suggesting that the site is strongly influenced by  $\text{NO}_x$ -rich local emissions. Concentrations of  $\text{HO}_2$  and  $\text{OH}$  radicals at Pasadena at noon are predicted to be among the lowest in the basin. Here,  $\text{NO}_x$  is depleting radicals. The isopleth for Pasadena shows an increase in peak ozone in response to decreased  $\text{NO}_x$  emissions over the widest range of control levels of any of the isopleths. The sensitivity to initial reductions in ROG is higher at Pasadena than at any of the other locations for which isopleths are shown. The ozone isopleth for downtown Los Angeles shows both a smaller increase with initial  $\text{NO}_x$  reductions and a smaller decrease with initial ROG reductions than the isopleth for Pasadena. Although like Pasadena, high concentrations of  $\text{NO}_x$  and ROG at 9 a.m. reflect strong local emissions at downtown Los Angeles, the value of  $\text{ROG}/\text{NO}_x$  predicted for downtown at noon is 21 ppm C/ppm.  $\text{HO}_2$  and  $\text{OH}$  concentrations are also predicted to be higher downtown than at Pasadena.

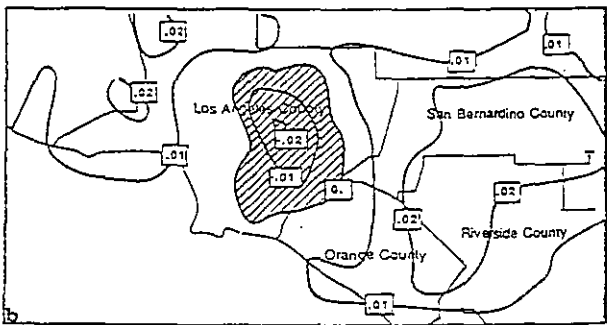
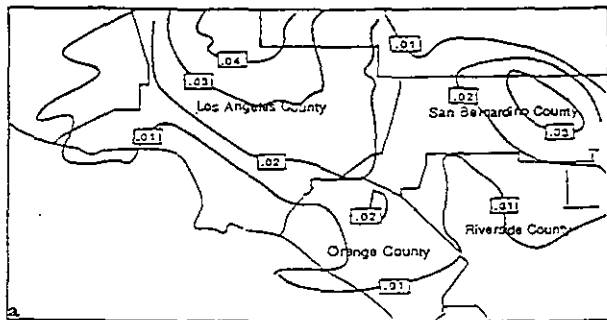


**Figure 7.** Spatial distribution of the predicted reduction in peak ozone concentrations (ppm) resulting from (a) a 35% reduction in ROG emissions and (b) a 35% reduction in  $\text{NO}_x$  emissions. Areas where ozone concentrations were predicted to increase with emissions reductions are cross-hatched; the associated concentration changes are shown as negative values.

Moving east out of Los Angeles County, the level of local emissions decreases and the influence of transported precursors becomes significant. ROG to  $\text{NO}_x$  ratios at noon at Chino, Rubidoux, and San Bernardino are predicted to exceed 25 ppm C/ppm.  $\text{HO}_2$  concentrations predicted for the same time and locations are about an order of magnitude higher than those predicted for Pasadena. The corresponding difference in OH concentrations is a factor of  $\sim 2$ . A progression from the significant negative sensitivity of ozone to  $\text{NO}_x$  emissions at Pasadena to the high positive sensitivity to  $\text{NO}_x$  at Rubidoux and San Bernardino is shown in the isopleths for these locations. The availability of  $\text{NO}_x$  is increasingly limiting ozone production. Consistent with higher radical levels in the air parcels passing over Rubidoux, the isopleth diagram constructed for that location displays less sensitivity to ROG emissions than those for San Bernardino and Chino.

Figure 7a shows the spatial distribution of the change in peak ozone concentration that results from a uniformly applied 35% reduction in ROG emissions, with  $\text{NO}_x$  emissions fixed at the base-line level. Figure 7b shows analogous results for a 35% reduction in  $\text{NO}_x$  emissions with no change in ROG. Comparison of the spatial patterns in Figure 7, parts a and b, with those of the parameters plotted in Figure 6 shows the correspondence of the peak ozone response to the balance that developed between ROG or radicals and  $\text{NO}_x$ . The change in  $\text{O}_3$  predicted to result from a 35% change in ROG is above 0.02 ppm throughout most of Los Angeles County, where base case  $\text{HO}_2$  concentrations were below  $0.1 \times 10^{-4}$  ppm at noon and OH concentrations were less than  $0.12 \times 10^{-6}$  ppm. The predicted change in  $\text{O}_3$  with ROG falls below 0.01 ppm over Riverside County, where  $\text{HO}_2$  concentrations exceeded  $0.5 \times 10^{-4}$  ppm.

The trend among the isopleths of generally increasing sensitivity to  $\text{NO}_x$  emissions, moving away from the high emissions area, corresponds to trends in the base case as well. In Los Angeles County, where base case  $\text{HO}_2$  and OH concentrations were less than  $0.1 \times 10^{-4}$  and  $0.1 \times 10^{-6}$

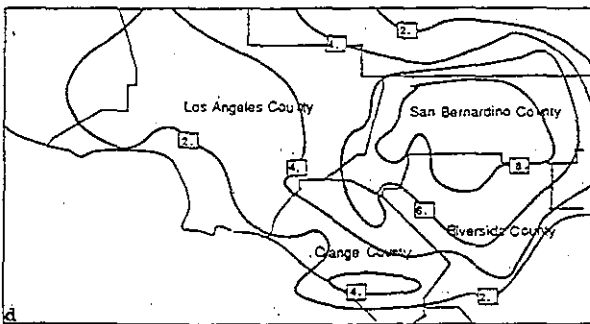
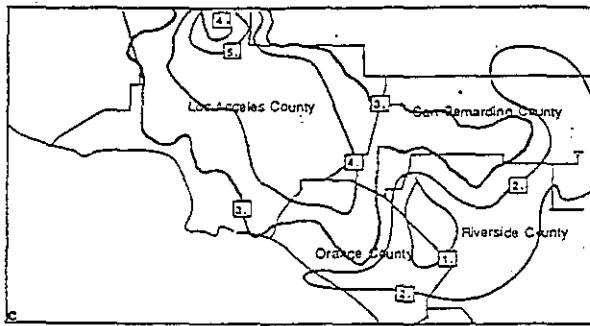
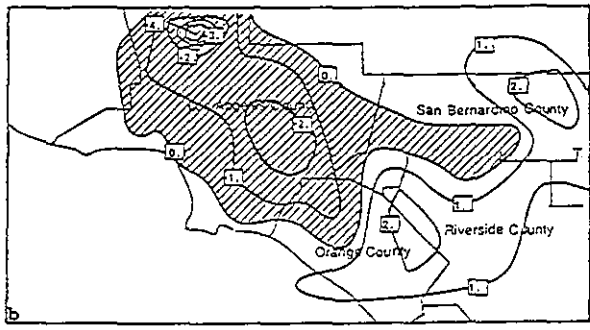
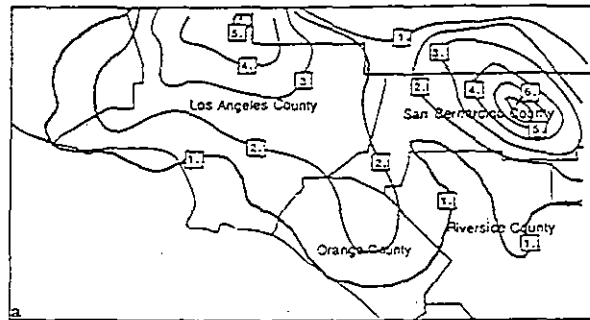


**Figure 8.** Spatial distribution of the predicted reduction in peak PAN concentrations (ppb) to (a) a 35% reduction in ROG emissions and (b) a 35% reduction in  $\text{NO}_x$  emissions, and of peak  $\text{NO}_3$  concentrations (ppb) to (c) a 35% reduction in ROG emissions and (d) a 35% reduction in  $\text{NO}_x$  emissions. Areas where product concentrations were predicted to increase with emissions reductions are cross-hatched; the associated concentration changes are shown as negative values.

ppm, and ROG/ $\text{NO}_x$  values remained below  $\sim 25$  ppm C/ppm until noon, peak ozone concentrations are predicted to increase up to  $\sim 0.02$  ppm in response to  $\text{NO}_x$  controls. East of there, radical concentrations and ROG/ $\text{NO}_x$  ratios in the base case were higher, and reductions in ozone concentration up to 0.025 ppm are predicted to result from a 35% decrease in  $\text{NO}_x$  emissions.

In summary, our analysis indicates that for the particular episode and for locations more than  $\sim 4$  h travel time downwind of downtown Los Angeles, reducing  $\text{NO}_x$  emissions also reduces  $\text{O}_3$  concentrations. For locations beyond  $\sim 8$  h downwind, where the highest ozone concentrations were observed,  $\text{NO}_x$  controls are more effective than ROG reductions. These results follow from the

**Figure**  
concentrations  
and of  
and (d)

chemis  
 $\text{NO}_x$  is  
Since  
 $\text{NO}_x$  r  
contro  
assum

7. Sp

PAN  
critical  
(27).  
portan  
duction  
ozone,  
sphere  
spatial  
35% c  
Figure  
effecti  
cantly

The  
similar  
in incr  
for ozo  
by 35%  
eastern  
to the  
Again  
to RO  
San B  
their c  
availa  
tion. I  
 $\text{NO}_x$  e  
peroxy  
oxidati  
PAN  
patter  
level o  
before  
 $\text{NO}_x$ -li

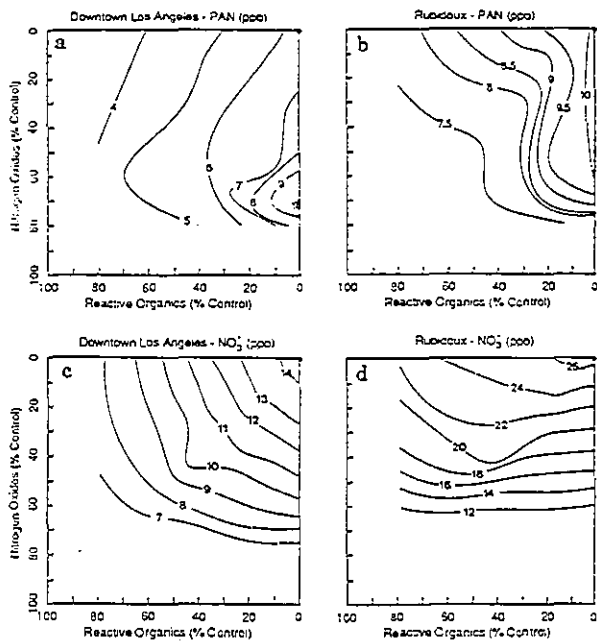


Figure 9. Predicted response to emissions reductions of peak PAN concentrations (ppb) at (a) downtown Los Angeles and (b) Rubidoux, and of peak  $\text{NO}_3^-$  concentrations (ppb) at (c) downtown Los Angeles and (d) Rubidoux.

chemistry of the  $\text{NO}_x$  and ROG cycles, and the fact that  $\text{NO}_x$  is removed from the system more rapidly than ROG. Since downtown Los Angeles has a lower typical ROG/ $\text{NO}_x$  ratio than most cities, the results suggest that  $\text{NO}_x$  control may generally be more effective than previously assumed.

### 7. Spatial Patterns in PAN and $\text{NO}_3^-$ Response

PAN, nitric acid, and aerosol nitrate concentrations are critical aspects of overall air quality in the Los Angeles area (27). Aerosol nitrate, in particular, has become more important from a regulatory point of view since the introduction of federal and state standards for  $\text{PM}_{10}$ . Like ozone, concentrations of these species in polluted atmospheres are modulated by  $\text{NO}_x$  and ROG emissions. The spatial distributions of the responses of PAN and  $\text{NO}_3^-$  to 35% changes in  $\text{NO}_x$  and ROG emissions are shown in Figure 8. For these species, as for ozone, the comparative effectiveness of  $\text{NO}_x$  and ROG reductions differs significantly across the airshed.

The response patterns for PAN and ozone are quite similar, except that the area where  $\text{NO}_x$  reductions result in increased peak concentrations is larger for PAN than for ozone. As with ozone, when  $\text{NO}_x$  emissions are reduced by 35%, the resulting reductions predicted for PAN at the eastern portion of the basin are comparable in magnitude to the predicted increases in the high emissions area. Again like the  $\text{O}_3$  response, PAN levels are most sensitive to ROG reductions in northern Los Angeles and western San Bernardino Counties. The similarity follows from their chemistry, since both PAN and  $\text{O}_3$  depend on the availability of peroxy radicals and  $\text{NO}_x$  for their production. PAN concentrations can be reduced by increasing  $\text{NO}_x$  emissions, leading to an enhanced rate at which peroxy radicals are reduced to hydroxyl radicals (via  $\text{NO}$  oxidation), an effect that favors  $\text{HNO}_3$  production over PAN production. The variation between the spatial patterns of PAN and ozone results from a difference in the level of depletion of  $\text{NO}_x$  relative to ROG that is required before production of the respective species becomes  $\text{NO}_x$ -limited.

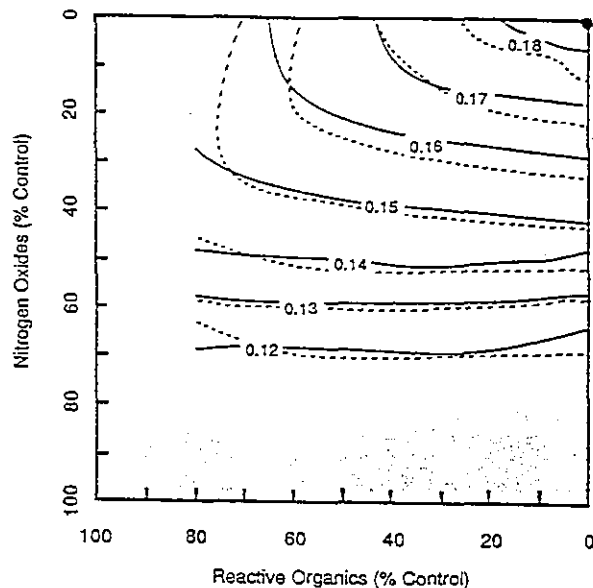


Figure 10. Response of the peak ozone concentration (ppm) at Rubidoux predicted with the trajectory formulation of the model with (—) the default chemical mechanism and (---) the "condensed" chemical mechanism of Lurmann et al. (28).

The  $\text{NO}_3^-$  response contours follow the base case concentrations of OH and  $\text{NO}_x$  closely and differ somewhat from those for  $\text{O}_3$  and PAN. The sensitivity of  $\text{NO}_3^-$  to ROG is highest where  $\text{NO}_x$  concentrations are highest, in Los Angeles County and western San Bernardino County. The patterns of sensitivity of  $\text{NO}_3^-$  to  $\text{NO}_x$  follow the contours of OH concentration, consistently increasing east across the basin. These results follow simply from the nitric acid formation reaction, with enhanced dependence on ROG for radical production where  $\text{NO}_x$  concentrations are high, and enhanced demand for  $\text{NO}_x$  where OH radical concentrations are elevated.

Figure 9 shows response surface isopleths for PAN and  $\text{NO}_3^-$  constructed for both downtown Los Angeles and Rubidoux. Peak base-line concentrations of both PAN and  $\text{NO}_3^-$  are predicted to be approximately twice as high at Rubidoux as at downtown. These two locations were selected so that both  $\text{NO}_x$ - and ROG-rich areas would be represented. As shown in Figure 9, parts a and b, the peak concentration of PAN would apparently be reduced more effectively by ROG than by  $\text{NO}_x$  reductions at both sites. As Rubidoux, however, the most effective means of reducing PAN may be a combination of  $\text{NO}_x$  and ROG reductions.  $\text{NO}_x$  and ROG reductions appear to be comparably effective in reducing  $\text{NO}_3^-$  at downtown Los Angeles (Figure 9c). At Rubidoux,  $\text{NO}_x$  emissions reductions are predicted to be significantly more effective in reducing  $\text{NO}_3^-$ , as shown in Figure 9d.

### 8. Effect of Model Formulation

Since the chemical mechanism used in the airshed model was developed several years ago, it is of interest to compare the results presented above with results generated with a more recent mechanism. As it was not feasible to perform the comparison with the full, Eulerian formulation, a trajectory version of the model was used. Since generating pollutant isopleths with an airshed model is not always practical due to computational requirements, it is also of interest to compare the Eulerian and Lagrangian results.

The isopleths presented in Figure 10 show the response of the  $\text{O}_3$  concentration predicted at Rubidoux to reductions in ROG and  $\text{NO}_x$  emissions. The isopleths were generated by two different mechanisms: the mechanism

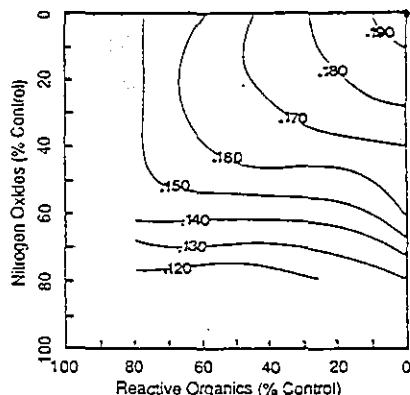


Figure 11. Response to emissions reductions as measured by the maximum peak ozone concentration (ppm) over the airshed.

employed in the calculations discussed previously, and the "condensed" chemical mechanism presented in Lurmann et al. (28). With each mechanism, the Lagrangian formulation of the model of McRae et al. (21-23) was used to follow a 2-day trajectory that passed through Rubidoux at 3 p.m. on August 31. Rubidoux was selected as the trajectory end point because it was near the location at which the airshed maximum  $O_3$  concentration was observed on August 31. The trajectory was developed from surface wind velocities measured at 39 sites, interpolated to 10-min time steps by the method of Goodin et al. (29). The initial conditions used are those given in Table I. Wind shear was not significant during the period (30). The response surfaces developed with the two mechanisms are quite similar, differing primarily at very large (greater than 75%) reductions in ROG emissions. A detailed comparison of the two reaction schemes is presented elsewhere (31).

The trajectory-generated isopleths presented in Figure 10 can be compared to the airshed results presented in Figure 4 for Rubidoux. Predicted  $O_3$  concentrations at varying ROG and  $NO_x$  levels agree closely between the airshed model and both trajectory formulations, with the airshed model generally predicting concentrations that are ~5% lower. Although the trajectory-generated isopleths show a small but distinct region of insensitivity to  $NO_x$  emissions levels, the major conclusion is confirmed: on the basis of equivalent fractional reductions,  $NO_x$  controls are predicted to be much more effective than ROG controls. The results further suggest that Lagrangian trajectory formulations can give results that are consistent with those of an Eulerian grid model. However, Eulerian and Lagrangian models can only be expected to agree under conditions of low wind shear, and if sufficient vertical resolution is included in the trajectory model to realistically treat deposition at the surface and entrainment of pollutants carried aloft above the morning inversion layer. A disadvantage of using a trajectory formulation is that if the location of the ozone peak shifts, as is likely with large emission changes, no indication is given of the shift, or of the location of the new maximum.

### 9. Implications for Control Strategies

The results presented in the previous sections show mixed responses to both  $NO_x$  and ROG controls.  $NO_x$  emissions reductions up to ~50% are predicted to lead to increased peak ozone and PAN concentrations over part of Los Angeles County, while ROG emissions reductions lead to decreased  $O_3$  and PAN concentrations across the region. The results for ozone are consistent with previous modeling studies that have considered the impact of relatively modest reductions in  $NO_x$  and ROG emissions

(17-19). The present analysis further indicates that  $NO_x$  reductions are necessary, alone or in combination with ROG controls, in order to reduce  $HNO_3$  and inorganic nitrate concentrations across the airshed.

The isopleth diagram presented in Figure 11 shows the airshed maximum 1-h average ozone concentrations corresponding to  $NO_x$  and ROG emissions reductions. Unlike an EKMA diagram, the airshed response surface reflects changes in the location of the maximum concentration, as emissions are reduced. Use of an airshed model allows this shift to be predicted and incorporated into the design of control strategies. As stated above, the highest 1-h ozone concentration predicted in the base case run is 0.20 ppm, predicted to occur at 3 p.m. near San Bernardino. With 25% reductions in  $NO_x$  or ROG or 15% reductions in both, the location at which the maximum is predicted to occur moves to the Chino area. This latter area is the location of the maximum concentrations predicted for the remainder of the model runs, except for those conducted for control combinations consisting of very large  $NO_x$  and small ROG reductions. For these cases, the airshed maxima are predicted to occur at the eastern edge of the modeling region and are influenced by flow reversals at night.

Following the standard EKMA approach, the control requirement for the Los Angeles area would be determined by moving from the base case emissions point (the upper right corner of the diagram) left along the upper edge of the diagram to the isopleth corresponding to the NAAQS of 0.12 ppm. In Figure 11, however, reductions in ROG emissions of up to 80% do not intersect the isopleth corresponding to 0.12 ppm. For the episode simulated, it appears impossible to reduce the airshed maximum ozone concentration below the standard by reducing ROG emissions, without substantial concurrent reductions in  $NO_x$ . This is due to the influx of organics from the northern and eastern boundaries. Inclusion of biogenic emissions would decrease the apparent effectiveness of ROG control further.

In addition to the need to consider  $NO_x$  control measures along with ROG controls, the response of the airshed maximum ozone concentration illustrates the probable infeasibility of the control problem (1, 2) presented above. In Los Angeles, for example, the 1982 Air Quality Maintenance Plan (AQMP) (19) identified available control steps that were expected by 1987 to reduce ROG emissions by 195 tons per day, at a cost approaching \$500 000 per day. The projected emissions reductions totaled only ~25% of the amount estimated to be required to achieve the NAAQS. The existence of such a shortfall suggests a cost effectiveness formulation of the control problem:

$$\begin{aligned} & \text{Max} \\ & \{E_{\text{ROG}}(x, t), E_{\text{ROG}}(x, t)\} \\ & \text{Air Quality } [E_{\text{ROG}}(x, t), E_{\text{NO}_x}(x, t)] \end{aligned} \quad (3)$$

subject to

$$\text{Cost}[\Delta E_{\text{NO}_x}, \Delta E_{\text{ROG}}(x, t)] \leq \text{Budget} \quad (4)$$

where Air Quality (3) is, in general, a vector of objective functions associated with different pollutant species or receptor areas. Analysis of the multiobjective control problem requires either a priori specification of weights or priorities among the objectives, or selection on the basis of calculated tradeoffs between alternative solutions.

The utility of focusing the analysis of control options on the airshed maximum ozone concentration is that it provides a single measure of the air quality in the basin on which decisions can be based. Especially when re-

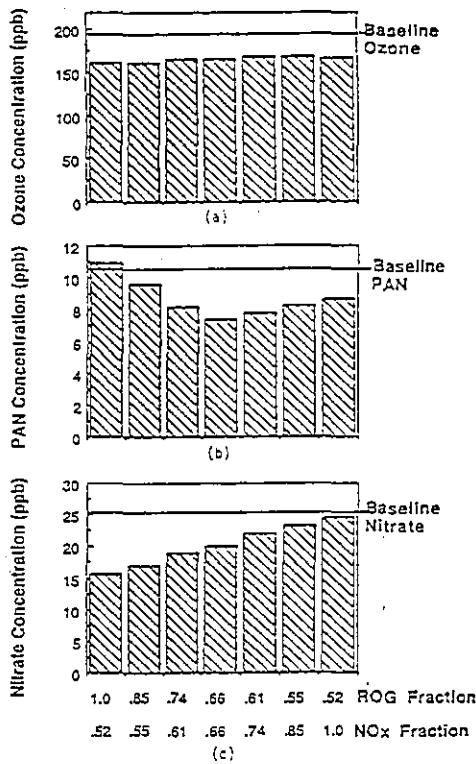


Figure 12. Ozone, PAN, and inorganic nitrate concentrations resulting from controlling ROG and NO<sub>x</sub> emissions to the levels indicated.

sources are limited, however, it is not clear that decisions should be made without considering changes in air quality at locations other than the location at which the maximum is observed. For example, under some control strategies the extent of the area over which concentrations exceed the NAAQS might increase, even as the value of the maximum concentration in the airshed is reduced. Furthermore, it may be beneficial to consider the impact of controls on concentrations of other pollutant species of concern, in addition to ozone. None of these issues can be addressed with the conventional EKMA methodology.

Figure 12 illustrates the tradeoffs predicted to exist between the level of reduction of PAN, NO<sub>3</sub>, and O<sub>3</sub> concentrations that can be achieved by using various combinations of NO<sub>x</sub> and ROG emissions controls. For PAN and inorganic nitrate, the concentrations plotted in Figure 12 were predicted for Rubidoux and are from Figure 9. In the base case, concentrations of these species at Rubidoux approached the highest predicted to occur anywhere in the airshed. The ozone concentrations plotted in Figure 12 are the airshed maxima for the control combinations indicated. Estimates presented in the 1982 AQMP for Los Angeles indicate that the costs of proportionate reductions in NO<sub>x</sub> and ROG emissions are comparable (e.g., the cost of a 10% reduction in NO<sub>x</sub> emissions is approximately equal to the cost of a 10% reduction in ROG emissions) and that costs increase roughly as the square of the reduction level (19). The control combinations for which reductions are shown in Figure 12 have thus been chosen to be roughly equal in cost to 50% reductions in either ROG or NO<sub>x</sub> emissions alone.

Clearly, the control combinations predicted to yield the largest reductions for each of the three pollutants are different. A striking aspect of Figure 12 is the flatness of the ozone curve, which contrasts with significant tradeoffs shown for PAN and inorganic nitrate. NO<sub>3</sub> is most effectively controlled by a pure NO<sub>x</sub> strategy. In contrast, concentrations of PAN can most effectively be reduced with a balanced combination of ROG and NO<sub>x</sub> controls.

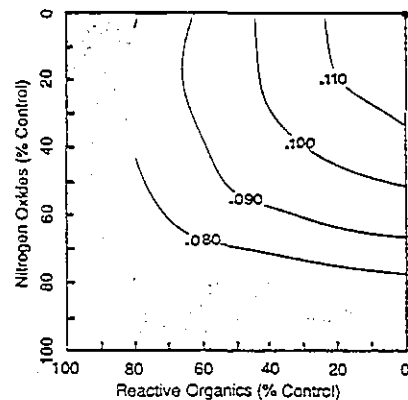


Figure 13. Response to emissions reductions as measured by the average peak ozone concentration (ppm) over the airshed.

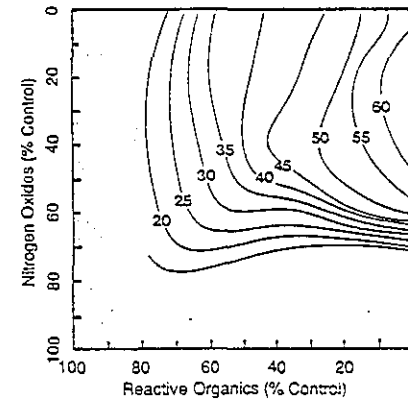


Figure 14. Response to emissions reductions as measured by the percent of the population within the modeling region exposed to ozone concentrations above 0.120 ppm.

With no basis for disregarding either pollutant, the question that still remains is how to trade off the reductions that could be obtained for inorganic nitrate and PAN.

The preceding example highlights a potential problem with U.S. EPA's current policy on photochemical air pollutants. On the basis of studies that examined the response of ozone, PAN, nitric acid, and other related pollutants to ROG reductions (32), U.S. EPA concluded that ozone is an adequate surrogate for the other photochemical pollutants of concern, i.e., that the other pollutants do not need to be treated explicitly (27). When both ROG and NO<sub>x</sub> controls are under consideration, however, U.S. EPA's assumption may not be adequate.

Tradeoff curves could be generated for various receptor locations as well as different pollutants. An alternative approach, which is especially useful when a single pollutant such as ozone is being considered, is to base control decisions on an air quality metric that is integrated over the region. Figures 13 and 14 present examples based respectively on giving equal weight to all grid cells in the modeling region and on the number of people residing in each grid cell. The predicted response of the airshed average peak ozone concentration shown in Figure 13 was estimated by

$$\text{Air Quality} = \frac{1}{A} \int_A \max_t [O_3(x, t)] dA \quad (5)$$

with A denoting the modeling region. Figure 14 shows how the fraction of the population potentially exposed to ozone levels above the NAAQS changes with NO<sub>x</sub> and ROG emissions, calculated as

$$\text{Air Quality} = \int_A \text{pop}(x) \delta(\max_t[\text{O}_3(x, t)]) dA \quad (6)$$

where

$$\delta(\max_t[\text{O}_3(x, t)]) = \begin{cases} 1 & \text{if } \max_t[\text{O}_3(x, t)] \geq 0.12 \text{ ppm} \\ 0 & \text{if } \max_t[\text{O}_3(x, t)] < 0.12 \text{ ppm} \end{cases} \quad (7)$$

Expression 6 obviously gives only a rough estimate of the fraction of people who would actually be exposed to ambient concentrations above the standard, since it ignores the factors of population mobility and indoor/outdoor concentration differences.

For the base case, the airshed average peak ozone concentration predicted by the model was 0.12 ppm. Figure 13 shows that the spatially averaged peak concentration is less sensitive to both  $\text{NO}_x$  and ROG reductions than peak concentrations at most specific locations. Similar in shape to the isopleths developed for San Bernardino and Chino, the airshed average isopleth shows fairly symmetric regions of relative insensitivity to  $\text{NO}_x$  and to ROG.

For the day modeled, at the base-line emissions level, almost 60% of the 10.8 million people living within the modeling region are estimated to be "exposed" to ozone concentrations above 0.12 ppm. As shown in Figure 14, with 50% reductions in both  $\text{NO}_x$  and ROG emissions, ~40% of the population is still predicted to be exposed. The exposure isopleth of Figure 14 is similar to the concentration isopleths developed for downtown Los Angeles and Pasadena, showing a significant region of the isopleth where  $\text{NO}_x$  reductions are predicted to increase the number of people exposed. The influence of the large population in the high emissions area is clearly reflected in this result, which is subject to change with the population growth projected to occur in the eastern SoCAB.

Numerous other integrated air quality metrics could be derived to indicate the effects of various control combinations for human health or agricultural or environmental damage. Which metrics are most appropriate for addressing the concerns and conditions of a specific air quality control area is a difficult question. The examples presented in this section suggest, on the basis of emissions/air quality relationships, that the answer will be a significant factor in determining which combination of ROG and  $\text{NO}_x$  controls appears most effective. The apparent efficacy of the control alternatives further depends on the level of control assumed to be feasible. A control strategy designed to minimize the number of people exposed to ozone concentrations above 0.12 ppm might utilize only ROG controls because moderate control of  $\text{NO}_x$  appears counterproductive. In contrast, if the objective is to reduce the airshed maximum concentration of ozone as much as possible, within the limits of available control measures, or to reduce  $\text{PM}_{10}$ , some degree of  $\text{NO}_x$  control might be desirable. Short of attaining the NAAQS, the airshed maximum ozone concentration predicted to result from alternative equal-cost combinations of ROG and  $\text{NO}_x$  reductions appears relatively insensitive to the combination of ROG and  $\text{NO}_x$  controls used, for the episode modeled. In such a case the responses of pollutants other than ozone might be used to select a control strategy.

## 10. Summary and Conclusions

This article has presented the results of a modeling study of the response of photochemical pollutant concentrations to ROG and  $\text{NO}_x$  emissions reductions. For the conditions modeled, the effects of ROG and  $\text{NO}_x$  emissions controls are predicted to differ significantly across receptor locations. Increases in ozone concentration with  $\text{NO}_x$

emission reductions are predicted for locations within the high emissions region of the airshed. As receptor sites further downwind are considered, basin-wide  $\text{NO}_x$  controls appear more effective. Reductions in  $\text{NO}_x$  emissions from the base level increase peak ozone concentrations at locations within 3-4 h travel time downwind of downtown Los Angeles, and lower peak ozone concentrations beyond that. ROG controls are predicted to be most effective in those areas where high  $\text{NO}_x$  levels are maintained and radical concentrations suppressed through midday.

Predicted patterns of response of PAN concentrations to  $\text{NO}_x$  and ROG emission reductions over the airshed approximately follow the response patterns for ozone.  $\text{NO}_3^-$  responses follow base-line  $\text{NO}_x$  and OH levels. Combined ROG and  $\text{NO}_x$  controls yield the greatest reductions in PAN concentrations.  $\text{NO}_x$  emissions controls are most effective in reducing  $\text{NO}_3^-$  concentrations. For the Los Angeles area, the question of whether a particular combination of ROG and  $\text{NO}_x$  control measures is robust over different types of meteorological conditions is an important area for further analysis. Additionally, the impacts of controls would be expected to be different if a future-year emissions inventory was used, or a specific set of control measures analyzed, rather than the uniform reductions considered here.

The results presented here call into question the commonly employed assumption that ROG emissions reductions are more effective in reducing ozone concentrations than reducing  $\text{NO}_x$ . Our analysis indicates that for the day considered, the NAAQS for ozone could not be met across the Los Angeles airshed without substantial reductions in  $\text{NO}_x$ . Moreover, the analysis indicates that a strategy of controlling  $\text{NO}_x$  emissions in combination with ROG emissions would help reduce ozone, PAN, and inorganic nitrate simultaneously.

This study has illustrated the importance of clearly defining the objectives of a control program. Isopleths depicting the effect of controls on the airshed maximum and spatially averaged peak ozone concentrations, and on the fraction of the population "exposed" to concentrations above the standard, suggest control strategies that differ not only in magnitude but also in "direction", in terms of the combination of ROG and  $\text{NO}_x$  emissions reductions indicated. Although different responses to ROG and  $\text{NO}_x$  controls will be seen for areas other than the Los Angeles basin, the conclusion is expected to hold elsewhere that the control combination judged to be most beneficial can depend strongly on the receptor locations, pollutants, measures of effectiveness, and degree of control considered. Guidance is needed from policymakers on how to make tradeoffs such as those illustrated here.

Registry No. PAN, 2278-22-0;  $\text{NO}_x$ , 11104-93-1;  $\text{O}_3$ , 10028-15-6;  $\text{HO}_2$ , 3170-83-0; OH, 3352-57-6.

## Literature Cited

- (1) Economic Report of the President. U.S. Government Printing Office, Washington, DC, January 1989.
- (2) Lioy, P. J.; Vollmuth, T. A.; Lippmann, M. J. *Air Pollut. Control Assoc.* 1985, 35, 1068-1071.
- (3) Kulle, T. J.; Sauder, L. R.; Hebel, J. R.; Chatham, M. D. *Am. Rev. Respir. Dis.* 1985, 132, 36-41.
- (4) Office of Air Quality Planning and Standards. Review of the National Ambient Air Quality Standards for Ozone. Staff Paper, U.S. Environmental Protection Agency, Research Triangle Park, NC, November 1988.
- (5) Thomas, L. M. Keynote Address, 79th Annual Meeting of the Air Pollution Control Association, Minneapolis, MN, June 22-27, 1986 *J. Air Pollut. Control Assoc.* 1986, 36, 997.

- (6) Office of Technology Assessment, Urban Ozone and the Clean Air Act: Problems and Proposals for Change. U.S. Government Printing Office, Washington, DC, April 1988.
- (7) Schwartz, S. E. *Science* 1989, 243, 753-763.
- (8) Meyer, E. L. Review of Control Strategies for Ozone and their Effects on Other Environmental Issues. EPA-450/4-85-011; U.S. Environmental Protection Agency, Research Triangle Park, NC, August 1986.
- (9) Gipson, G. L.; Freas, W.; Kelly, R.; Meyer, E. Guideline for Use of City-Specific EKMA in Preparing Ozone SIPs. EPA-450/4-80-027; U.S. Environmental Protection Agency, Research Triangle Park, NC, 1981.
- (10) Baugues, K. A Review of NMOC, NO<sub>x</sub> and NMOC/NO<sub>x</sub> Ratios Measured in 1984 and 1985. EPA-450/4-86-015; U.S. Environmental Protection Agency, Research Triangle Park, NC, 1986.
- (11) Sillman, M. S. Models for Regional-Scale Photochemical Production of Ozone. Ph.D. Thesis, Harvard University, Cambridge, MA, 1987.
- (12) Trainer, M.; Williams, E. J.; Parrish, D. D.; Buhr, M. P.; Allwine, E. J.; Westberg, H. H.; Fehsenfeld, F. C.; Liu, S. C. *Nature* 1987, 329, 705-707.
- (13) Chameides, W. L.; Lindsay, R. W.; Richardson, J.; Kiang, C. S. *Science* 1988, 241, 1473-1475.
- (14) Lindsay, R. W.; Richardson, J.; Chameides, W. L. *JAPCA* 1989, 39, 40-43.
- (15) U.S. Environmental Protection Agency. *Fed. Regis.* November 17, 1987.
- \* (16) Shafer, T. B.; Seinfeld, J. H. *Atmos. Environ.* 1986, 20, 487-499.
- \* (17) Russell, A. G.; McCue, K. F.; Cass, G. R. *Environ. Sci. Technol.* 1988, 22, 1336-1347.
- (18) Rao, S. Application of the Urban Airshed Model to the New York Metropolitan Area. EPA-450/4-87-011; U.S. Environmental Protection Agency, Research Triangle Park, NC, 1987.
- (19) South Coast Air Quality Management District. Final Air Quality Management Plan: 1982 Revision. El Monte, CA, October 1982.
- (20) Seinfeld, J. H. *JAPCA* 1988, 38, 616-645.
- \* (21) McRae, G. J.; Goodin, W. R.; Seinfeld, J. H. *Atmos. Environ.* 1982, 16, 679-696.
- \* (22) McRae, G. J.; Seinfeld, J. H. *Atmos. Environ.* 1983, 17, 501-522.
- \* (23) Russell, A. G.; McCue, K. F.; Cass, G. R. *Environ. Sci. Technol.* 1988, 22, 263-271.
- (24) Russell, A.; Harris, J.; Milford, J.; St Pierre, D. Quantitative Estimate of the Air Quality Impacts of Methanol Fuel Use. Report to the California Air Resources Board, Sacramento, CA, 1989.
- (25) Horie, Y. Ozone Episode Representativeness Study for the South Coast Air Basin, Appendix V—P. Draft 1988 Air Quality Management Plan, South Coast Air Quality Management District, El Monte, CA, 1988.
- (26) U.S. Environmental Protection Agency. Uses, Limitations and Technical Basis of Procedures for Quantifying Relationships between Photochemical Oxidants and Precursors. EPA-450/2-77-021a; Research Triangle Park, NC, November 1977.
- (27) U.S. Environmental Protection Agency. Air Quality Criteria for Ozone and Other Photochemical Oxidants. EPA-600/8-84/020bF; Research Triangle Park, NC, August 1986.
- (28) Lurmann, F. W.; Carter, W. P. L.; Coyner, L. A. A Surrogate Species Chemical Reaction Mechanism for Urban-Scale Air Quality Simulation Models. EPA Contract No. 68-02-4104, May 1987.
- \* (29) Goodin, W. R.; McRae, G. J.; Seinfeld, J. H. *J. Appl. Meteorol.* 1979, 18, 761-771.
- \* (30) Russell, A. G.; Cass, G. R. *Atmos. Environ.* 1986, 20, 2011-2025.
- \* (31) Milford, J. B.; Russell, A. G.; McRae, G. J., submitted.
- (32) Altshuller, A. P. *Atmos. Environ.* 1983, 17, 2383-2427.

Received for review May 12, 1988. Revised manuscript received March 9, 1989. Accepted March 24, 1989. This work was supported by the National Science Foundation under a Presidential Young Investigator Award CEE000659 to G.J.McR. and by the PRECP program under Grant B-K5877-A-E from Battelle Pacific Northwest Laboratories. Computer time, facilities, and assistance were provided by the Pittsburgh Super Computing Center and Cray Research, Inc.